The coating application for enhanced adhesion between GFRP composites and cataphoresis-coated (KTL) steel – part 1: mechanical properties

Celalettin Baykara and Enes Bilgin
Technology Faculty, Sakarya University of Applied Sciences, Sakarya, Türkiye

Received 25 April 2025
Revised 12 May 2025
Accepted 13 May 2025

Abstract

Purpose – This research aims to investigate how the adhesion performance of GFRP composite components, commonly used in railway vehicles, is affected when bonded to cataphoresis coated steel substrate surfaces.

Design/methodology/approach – In this context, the aim was to determine the optimal adhesion parameters for bonding GFRP samples with natural and primed surfaces to steel samples with cataphoresis coatings. Then, single-lap joint samples with different bond thicknesses of 1 mm, 2 mm and 3 mm were prepared. Finally, tensile tests were performed on the samples.

Findings – The results showed that GFRP specimens with natural surfaces, characterised by the highest surface roughness, exhibited the lowest bond strength. But, the highest bonding performance was achieved in specimens where primed GFRP was bonded to cataphoresis coated steel, especially with a bond thickness of 1 mm, and achieving a yield strength of 20 MPa. This situation explains the characteristic difference between surface roughness and chemical coating, which are two essential pre-treatments in adhesive bonding. While surface roughness provides mechanical interlocking, excessive roughness can hinder the adhesive's wetting ability, causing it to remain suspended on the surface as described in the Cassie–Baxter theorem. In contrast, it has been observed that, despite low surface roughness, chemical coatings enhance the bonding between primer paint and adhesive molecules, and – as stated in the Wenzel theorem – improve the surface wettability.

Originality/value – As a preliminary preparation in the adhesive method, primer paint is applied to steel surfaces and GFRP material surfaces in classical industrial applications. In this research, the application of the catapheresis process to the steel substrate instead of primer paint and the bonding of primer-painted GFRP materials to this surface make a unique contribution to the research.

Keywords Adhesion bonding, Surface coating, Cataphoresis coating (KTL), Primer painting, Wenzel equation, Cassey–Baxter equation

Paper type Research paper

1. Introduction

Adhesive bonding has become increasingly important in lightweight engineering applications, especially in industries such as automotive, aerospace and railways, where the joining of different materials – such as polymers and metals – is required. Glass fibre-reinforced polymer (GFRP) composites are known for their high strength-to-weight ratio and corrosion resistance

This research was supported by the Sakarya University of Applied Sciences in the scope of Master's Thesis Project under project number 285–2025. In addition, the author would like to thank Mr. Necati Oğuz Sertsoz and Mr. Ramazan Ötemen, one of the experts from TURESAS-SAKARYA PLANT, for their technical supports, and also Mr. Koray Barutoğlu and Mr. Koray Özder, experts from Sika Türkiye A.Ş for the successful ageing tests within the scope of R&D.

Declaration of competing interest: The author declares that they have no known competing financial interests or personal relationships that could have appeared to influence the work reported in this paper.

Railway Sciences
Vol. 4 No. 4, 2025
pp. 425-449
Emerald Publishing Limited
e-ISSN: 2755-0915
p-ISSN: 2755-0907
DOI 10.1108/RS-04-2025-0012

and are often combined with metal components to integrate structural integrity with durability. However, achieving reliable adhesion between polymeric and metallic surfaces in adhesive bonding without proper surface preparation is a significant challenge. Surface properties, such as roughness, surface energy and chemical compatibility, directly influence the strength and stability of adhesive bonds. This study focuses on evaluating the effects of surface roughening and primer coating processes on the adhesion performance of GFRP–KTL steel joints in railway vehicles.

In modern railway transportation vehicles, the demand for lightweight vehicles in global transportation systems such as air, sea and land transportation is important for reducing the harmful environmental impacts of composite materials, increasing reliability, ease of repair, lowering production and service costs and enhancing competitiveness (Palomba, Epasto, & Crupi, 2021; Akniyet *et al.*, 2022; Fu *et al.*, 2019; Bi, Wang, Xu, & Li, 2022). Composite materials provide superiority over conventional steel materials due to high density/strength ratios, flexibility in design, superior resistance to high temperature and corrosion and fuel saving (Lin *et al.*, 2025; Price & Hull, 1987; Mamalis, Manolakos, Ioannidis, & Papapostolou, 2004; Farley, 1983). Composite materials refer to a material whose properties are enhanced as a result of the different benefits of each component as a result of the integration of at least two components, such as fibre and matrix with different properties and advantages (Rajak, Pagar, Kumar, & Pruncu, 2019).

In the train and wagon manufacturing industry, the adhesive bonding method is used for the assembly of composite components on the steel body for different material types. GFRP, one of the composite materials, plays an important role in the railway industry due to its lightweight structural properties. Traditionally, primer paint coatings have been used to improve bond strength on metal substrates. However, environmental concerns and the need for more efficient, durable bonding techniques have encouraged the investigation of alternative surface treatments. This study investigates the use of cataphoresis coating, a highly uniform and corrosion-resistant process, in place of conventional primer paint on steel surfaces. The adhesive bonding method provides many advantages over conventional joints, such as superior corrosion resistance, good strength-to-weight ratio, homogeneous stress distribution, impermeability and low production cost than conventional thermal and mechanical fastener joining methods (Banea & Da Silva, 2009; Barnes & Pashby, 2000; Guadagno *et al.*, 2015; Pethrick, 2015). Mechanical joints do not provide a homogeneous load transfer as they require drilling through the surface (Fischer *et al.*, 2012; Ozgür, Erhan, Onur, Belgin, & Arif, 2018; Fuertes, Kruse, Koerwien, & Geistbeck, 2015; Zhang, Shan, Tan, & Zhang, 2017; Kreling, Fischer, Delmdahl, Gäbler, & Dilger, 2013). In addition, additional weights such as rivets, bolts and thermal effects that may occur in methods such as welding are eliminated (Correia, Anes, & Reis, 2018). Adhesive joints prevent heterogeneous stress concentration by creating a homogeneous stress distribution (Nidhal, Yasmina, Sami, Salah, & Martins, 2023; Wang, Hao, Zhou, Li, & Hua, 2016; Wui *et al.*, 2021).

To ensure effective bond strength in adhesive joints, it is necessary to remove solid contaminants from the environment, to abrade the surface and to apply chemical pretreatments such as paint and coating to the material surfaces (Moreira, Oliveira, Silva, Vilar, & Moura, 2018; Oliveira, Moreira, Moura, & Vilar, 2018). While the surface roughening process increases the adhesion area on the material surface, it causes a mechanical lock effect between the material and the adhesive agent. Ghumatkar *et al.* investigated the effect of surface roughness on bonding strength by tensile test using epoxy adhesive on AISI 1045 steel and AA 6063 materials at various surface roughness levels. In conclusion, they identified the optimum surface roughness for both materials (Ghumatkar, Sekhar, & Budhe, 2017). Yuan *et al.* investigated the tensile strength of homogeneous surfaces of CFRP composite materials on different surfaces by mechanical methods using femtosecond lasers, which cause less surface damage, high precision and less surface damage. In consequence of this research, a high surface energy and surface polarity were achieved (Yuan, Guo, He, Zhang, & Han, 2024). Surface coatings of materials can be analysed in two basic groups: Firstly, a chemical coating

using primer paint pigments, secondly, electrochemical etching of material surfaces with techniques such as anodising and cataphoresis. As a result of applying primer paint or any chemical coating on the surface of all kinds of materials, such as metal, composite rubber, etc. the surface energy will increase and the binding elements will cause a superior wettability.

Primer painting, although surface preparation such as cleaning, sanding and filling surface defects such as cracks or gaps before any paint or coating process to be applied to the surface of a material, sometimes primer paint is applied before the paint or any surface coating process to be applied. Thus, a perfect chemical bond is formed between the primer paint and the topcoat paint to be applied and the topcoat paint manages to adhere to the primer paint. This improves the paint quality. The superior adhesion ability of the topcoat paint on the primer paint ensures that the adhesive agent also adheres perfectly on the primer paint. Primer paint increases the surface energy on the material and enables the adhesive agent to wet the material surface completely. For this reason, the primer plays an important role in the surface preparation phase of the adhesive method.

Cataphoresis coating is an electrochemical coating process and is used in conductive materials. This process is a critical production process in the automotive industry, such as primer paint, which is effective in increasing corrosion resistance. In such coatings, the formation of a thin chemical film on the surface is a parameter that increases the adhesion strength. In addition, surface coatings also prevent corrosion of metallic parts. Therefore, many researchers have investigated the effect of chemical preliminaries on adhesive strength by investigating different methods such as anodising processes (Zhang, Zhao, Zuo, & Xiong, 2008; Correia *et al.*, 2018; Molitor, Barron, & Young, 2001; He, Chen, Yu, Yue, & Yang, 2013), sol-gel (Cobb, Johnson, Lowther, & St Clair, 1999; Blohowiak, Osborne, & Krienke, 1998) and primer paint (Callinan & Galea, 2002; He, Huang, Fisher, Yue, & Yang, 2015). Recently, more environmentally friendly and different methods have started to be investigated. In this context, Ardila-Rodriguez *et al.* applied UV/ozone treatment to activate and improve the wettability of titanium alloy surfaces. As a result, it was found that the surface was more oxidised by this process, resulting in a lower contact angle and increased adhesion ability as a result of the end tension test (Ardila-Rodriguez *et al.*, 2021). Bloomfield investigated a two-part primer system based on cyanoacrylate, which enables strong adhesion of adhesives to silicone rubber. In conclusion, he stated that this primer forms a porous and nanostructured thin coating film that is firmly bonded to silicone. Baykara observed that cataphoresis-coated surfaces had better bond strength than primer-coated surfaces in experimental fatigue tests on single lap joint types with DC01A steel materials with primer and cataphoresis-coated surfaces (Baykara, 2023a, b; Baykara *et al.*, 2024). Baykara *et al.* observed that cataphoresis coating was effective in the fatigue test with DC01 A steels with primer and cataphoresis-coated surfaces by numerical analysis under the same conditions (Baykara, Teke, & Ertas, 2023). Rudawska and Wahab investigated the adhesive strength of AA 5754 alloy materials with catoferitic powder coating and primer coating on the surface. As a result, they observed that the catopherisis coating had an effect on the bond strength (Rudawska & Wahab, 2019).

GFRP materials are composite materials obtained by combining high-strength glass fibres with a thermoplastic and thermoset polymer resin matrix. Due to the superior strength and durability of the glass fibre and the flexibility and chemical resistance of the polymer resin, combined with its strength and corrosion resistance, it forms an engineering material that is frequently used in many industries such as automotive, aerospace, construction and marine (Alachek, Reboul, & Jurkiewiez, 2019). GFRP composites improve the aerodynamic structure of vehicles by producing geometrically difficult parts and save energy by reducing the transmission of heat and cold. Due to its high strength-low weight ratio, it contributes to fuel saving in internal combustion vehicles, reducing carbon footprint and increasing range in electric vehicles, and it is a sustainable material in the automotive sector due to its long service life and resistance to corrosion and low maintenance requirements. Examples of GFRP composite components used in train body production, which are formed by welding steel tubes

of different sizes, are the front/rear mask and bumper for the train (Figure 1) and wagon (Figure 2), some main trimming parts as side wall and ceiling coverings (Figure 3).

Ostapiuk and Bienias (2020) investigated the shear strength and fracture behaviour of Al/GFRP adhesive bonded joints. As a result, it was stated that a successful adhesive bond would be obtained by roughening the appropriate metal surfaces. Goudarzi and Khedmati (2020) investigated the adhesive bond strength experimentally and numerically in single and double lap joints of Al/GFRP materials with the adhesive method. As a result, they found 33% more bond strength in single lap joints than in double lap joints. Zamani, Jaamialahmadi, da Silva, and Farhangdoost (2019) investigated the crack initiation and fatigue life under static loading conditions in Al/GFRP material joining in single lap joints. As a result, they found that the crack initiation life was approximately half of the total life. Zamani, Jaamialahmadi, and Da Silva (2023) investigated the strain life criteria in single lap joints and Al/GFRP material combinations and investigated the fatigue life cycles in single lap joint types by numerical analysis method.

1.1 Surface roughness and mathematical modelling

The strength of adhesive bonding depends on various surface properties of the material, such as wettability and roughness. Surface roughness is an important parameter affecting the adhesion strength and wettability of material surfaces (Guo *et al.*, 2021). Studies have shown that an indefinite increase in surface roughness does not certainly increase the strength of adhesion. The initial increase in roughness increases the adhesion strength, then reaches a saturation plateau and starts to decrease for large roughness values (Liu *et al.*, 2022).

Gaussian distribution: Surface roughness was first established with the assumption of similarity to a Gaussian distribution (Greenwood & Williamson, 1966). It has been determined that surface roughness patterns affect the contact angle. These pattern profiles were examined

Figure 1. Front/rear mask and bumper for train. Source: Authors' own work

Figure 2. Front/rear mask for wagon. Source: Authors' own work

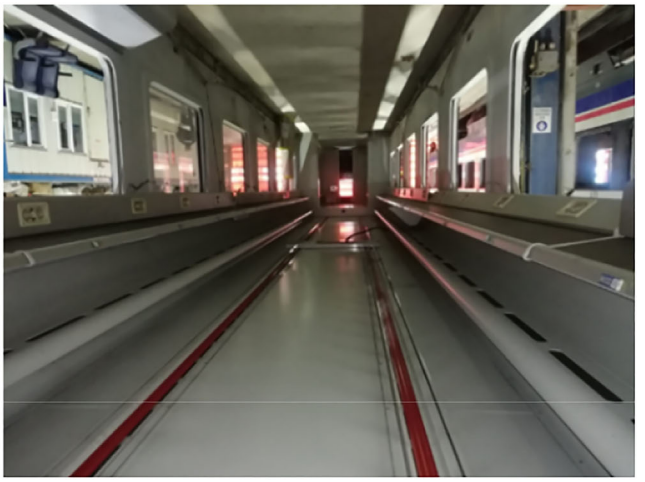

Figure 3. Side wall and celing cover. Source: Authors' own work

in an experimental study in triangular, square, hexagonal and octagonal sections, and it was determined that they play an important role in forming the contact angle (Kim *et al.*, 2020). A solid surface shows changes in wetting ability due to its different topographic microstructure. These changes have been reported as pillar-structured surfaces, pore-structured surfaces and groove-structured surfaces (Jiang & Choi, 2020). It has been stated that the depth and width ratios in the roughness microstructure of a solid surface are an effective

parameter in the contact angle. As this ratio increases, the wetting area increases and activates the contact angle (Cao *et al.*, 2021).

Young's theorem: The surface free energy of a liquid droplet on a smooth solid surface is stated by the Young equation (Equation (1)) as a function of the surface tension of the liquid and the interfacial tension between the liquid and solid phases, and the equilibrium between the solid, liquid and gas phases is defined by the contact angle (Equation (2)) (Figure 4).

$$\gamma_{sv} = \gamma_{sl} + \gamma_{lv} cos\,\theta_Y \tag{1}$$

$$cos\,\theta_Y = \frac{\gamma_{sv} - \gamma_{sl}}{\gamma_{lv}} \tag{2}$$

where

γ_{sv}: solid surface free energy

γ_{sl}: solid/liquid interfacial tension

γ_{lv}: liquid/air surface tension

θ_Y: Young contact angel

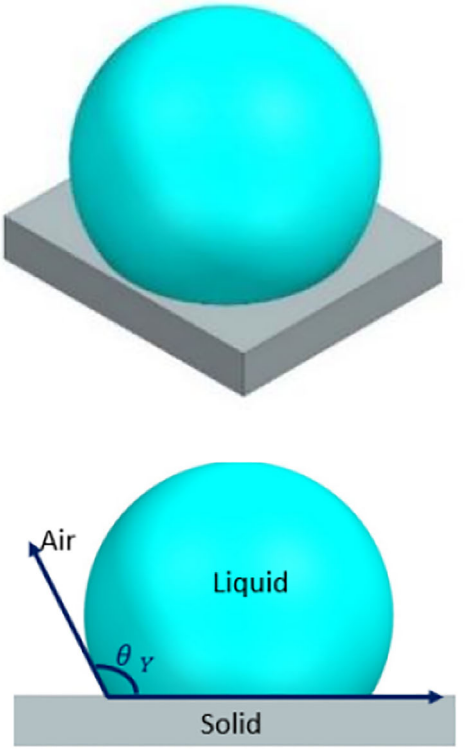

Figure 4. Wetting ability of a liquid drop on a surface according to the Young's theorem. Source: Authors' own work

The Young equation presumes that the surface is smooth and chemically homogeneous. In real industrial surfaces, any modification, such as surface roughness caused by any chemical coating or physical applications, changes the surface characteristic property. In this case, a contact angle that is in balance on a smooth surface will create a contact angle that increases and decreases due to the topographic feature of the rough surface, and the Young equation loses its validity.

Wenzel model: In the bonding method, one of the important preliminaries in the mechanical clamping theory is the surface roughness. The adhesive droplet contacts the rough surface, causing the pits on the surface to be completely wetted. Thus, the relationship between wettability and surface roughness is explained by Robert N. Wenzel, who modifies the Young's equation in Equations (1), (3) and (4), where the area of a rough surface where the solid and liquid phases are in contact is larger than the geometrical area (Equation (5)) (Figure 5).

$$cos\,\theta_Y = \frac{\gamma_{SV} - \gamma_{SL}}{\gamma_{LV}} \tag{3}$$

$$cos\,\theta_W = R_f . \left[\frac{\gamma_{SV} - \gamma_{SL}}{\gamma_{LV}}\right] \tag{4}$$

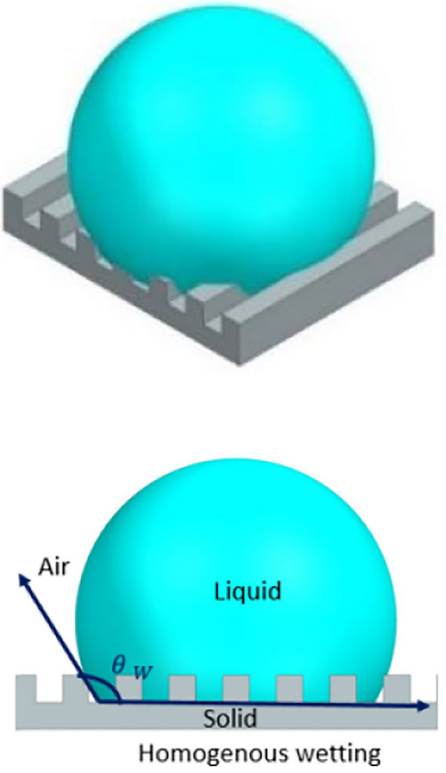

Figure 5. Wetting ability of a liquid drop on a surface according to Wenzel theorem. Source: Authors' own work

$$\cos\theta_W = R_f . \cos\theta_Y \tag{5}$$

where

θ_W: Actual measured contact angle in Wenzel model

θ_Y: Young's contact angle

R_f: Roughness ratio

The roughness ratio is defined as the ratio between the actual and the projected solid surface area (Equation (6)).

$$R_f = \frac{Actual\ area}{Projected\ area} \tag{6}$$

A correction factor which is defined as Rf is used when moving from a smooth surface to a rough surface to relate it to the actual equilibrium contact angle measured on a smooth surface in this model. This factor is directly related to the geometric area as a percentage increase of the actual area.

Cassie–Baxter model: If the surface is partially wetted by the droplet, in other words, if there are air gaps between the liquid and the solid, the Wenzel model may not be sufficient. In this case, the Cassie–Baxter model is more suitable. The Cassie–Baxter model assumes that the liquid droplet is suspended on the solid surface at the microscale and there is a composite interface between the two phases (Ghasemlou, Daver, Ivanova, & Adhikari, 2019). In this model, the measured contact angle is a function of the droplet area on the solid sample and the droplet area in air (Equation (7)) (Figure 6).

$$\cos\theta_{CB} = f_{sl} . \cos\theta_{sl} + f_{la} . \cos\theta_{la} \tag{7}$$

f_{sl}: Solid–liquid surface fraction

f_{la}: Liquid–air surface fraction

θ_{sl}: Solid–liquid contact angel

θ_{la}: Liquid–air contact angel

As seen in Figure 1, since the angle of the liquid-air interface is 180° and cos 180 = −1, when applied to Equations (7), (8) is obtained.

$$\cos\theta_{CB} = f_{sl} . \cos\theta_{sl} - f_{la} \tag{8}$$

The Wenzel and Cassie–Baxter models measure the static contact angle as a fraction of the solid phase area over the entire surface. The Wenzel model states that the roughness ratio is only valid for isotropic surfaces and frictional contact areas with uniform morphology (McHale *et al.*, 2007). It may not give a consistent result for heterogeneous surfaces with complex morphologies. Such heterogeneous structures are analysed as fractal geometry models. In this context, the solid surface energy and the microstructure of the contact line are found to be more important factors than the internal geometry of the contact area (Extrand, 2002).

In adhesive bonding processes, the surface characteristics of substrates are a critical parameter. The transition between the Wenzel and Cassie–Baxter theories, which describe the mechanisms of adhesion, has been extensively investigated by researchers in numerous studies. Hejazi *et al.* noted that the Wenzel and Cassie–Baxter models are widely used to explain the dependence of contact angle on rough and patterned solid surfaces; however, these two classical models do not always accurately predict surface wettability. These models

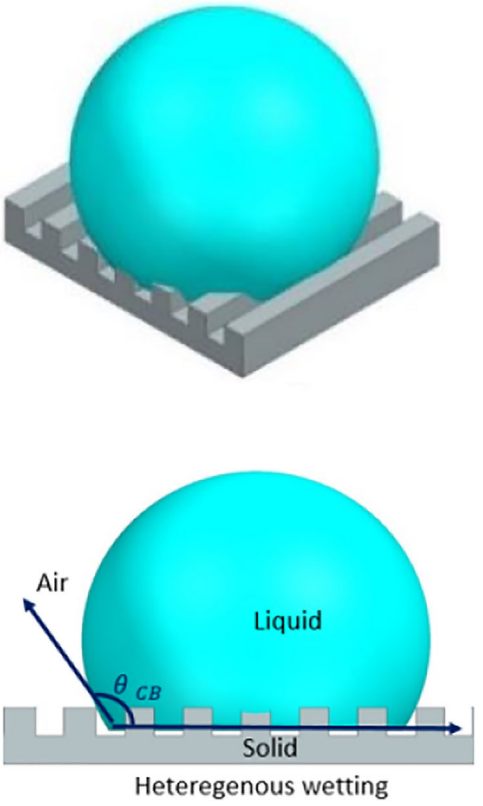

Figure 6. Wetting ability of a liquid drop on a surface according to Cassey-Baxter theorem. Source: Authors' own work

overlook many interactions that occur during wetting, such as discharge pressure, crystalline microstructure, grain boundaries and the presence of defects. Such influences are referred to as "secondary effects," and it has been demonstrated that discharge pressure can affect wettability through the formation of thin liquid films in the isotherm. In the study, water contact angles were measured on metal surfaces that had nominally the same Wenzel roughness, achieved through abrasion and chemical etching. These two surface roughening techniques produce different surface structures, leading to distinct contact angle values that cannot be fully explained by either the Wenzel or Cassie models. On stainless steel and aluminium alloy surfaces, chemical and physical changes caused by intergranular corrosion and selective dissolution of intermetallic phases result in nano- and microscale surface roughness (Hejazi, Moghadam, Rohatgi, & Nosonovsky, 2014). Sudeepthi *et al.* investigated an irreversible Cassie–Wenzel wetting transition on a nanostructured superhydrophobic surface induced by surface acoustic wave (SAW) vibration. The transition was achieved by the penetration of liquid into nanoservices, driven by the inertial energy imparted to the droplet by the SAW. However, the filling of the nanopores presents an energy barrier (Eb) that must be overcome, requiring the replacement of the initial solid–air interface with a solid–liquid interface. The study demonstrated that the occurrence of the wetting transition is governed by the relative magnitudes of the input acoustic energy (Eac) and this energy barrier. Furthermore,

the irreversibility of the transition was explained through the energy minimization of the system after the transition. By observing the dynamics of the wetting front, the different stages of the wetting transition process were also identified (Sudeepthi, Yeo, & Sen, 2020). Rauter *et al.* investigated how mass transfer across a liquid–ventilation transition membrane is influenced by the state of liquid–vapour interfaces on the membrane surface, pore geometry and solid–liquid interactions within the membrane. Mass flow was simulated across a gas-permeable membrane with liquid evaporation occurring on one side and condensation on the other. Simulations were conducted for both Wenzel-like and Cassie–Baxter-like states on each side of the membrane. The interaction between the liquid and the solid within the membrane varied between contact angles of 125° and 103°. For a constant driving force, the Cassie–Baxter state yielded nearly 40% higher mass flow compared to the Wenzel state. This difference was attributed to an insufficient supply of vapour particles at the pore entrance in the Wenzel state. However, the distinction between the Wenzel and Cassie–Baxter states diminished in cases where pore resistance increased (Rauter, Schnell, & Kjelstrup, 2021).

Khaskhoussi *et al.* designed superhydrophobic surfaces on AA6082 aluminium alloy using chemical etching in an HF/HCl solution followed by silanization through a self-assembly process, aiming for corrosion protection in marine environments. Various etching durations were investigated to optimize the surface treatment effects. The results demonstrated that all prepared surfaces exhibited superhydrophobic characteristics after silanization, with contact angles exceeding 150°. Both contact and sliding angles varied depending on surface morphology as influenced by the etching duration. The most optimal outcome was achieved with a 20-s etching period, which resulted in a coral-like microstructure and a homogeneous, well-ordered pixel-like nanostructure. This surface displayed Cassie–Baxter-type superhydrophobic behaviour, characterized by a water contact angle of 180° and a sliding angle of 0°. All superhydrophobic surfaces showed twice the corrosion protection efficiency and impedance modulus in simulated seawater compared to untreated AA6082 (Khaskhoussi, Calabrese, & Proverbio, 2022). Park *et al.* investigated the control of surface wettability through micro-conical structures inspired by the lotus leaf. These structures were fabricated on silicon substrates and then replicated onto PDMS, a flexible and transparent material. Contact angle measurements revealed that the surfaces exhibited superhydrophobic properties. Additionally, the study identified criteria governing the transition between the Cassie–Baxter and Wenzel states, demonstrating the feasibility of producing low-cost, elastic, transparent and water-repellent surfaces (Park, Ribe, Fernandino, & Dorao, 2023). Hure *et al.* investigated the mechanical effects of surface structures on ice adhesion, rather than evaluating it solely based on wettability on superhydrophobic surfaces. The results showed that in the Wenzel state, where ice penetrates into surface cavities, adhesion increased by 30%, whereas in the Cassie state, where air is trapped, adhesion decreased by 36%. Fracture toughness values were calculated for both states and validated through finite element modelling, demonstrating that a mechanical approach offers a more accurate prediction of ice adhesion behaviour (Huré, Olivier, and Garcia, 2022). Xin *et al.* investigated the Cassie–Wenzel (C–W) wetting transition and its mechanisms on water films over different surface topologies, including columnar-arranged and strip-patterned surfaces. On columnar-arranged surfaces, the free energy initially increases as water enters the gaps, but after contacting the substrate surface, it decreases, following a classic wetting path. In contrast, on strip-patterned surfaces, multiple partial wetting states are formed, each possessing a local energy minimum. Therefore, during the C–W transition, the water film must overcome several energy barriers. Additionally, the effects of the aspect ratio of both surfaces and their inherent wettability on this transition were also discussed (Xin He *et al.*, 2021). Xin *et al.* directly observed the dynamic wetting transitions of nanoscale water films on surfaces with dual-scale (hierarchical) roughness. Transitions between different wetting states, such as Cassie–Cassie, Wenzel–Cassie, Cassie–Wenzel and Wenzel–Wenzel, were analysed using atomistic simulations and sampling techniques. Two primary wetting pathways were identified: primary preferred entry and secondary entries. The pathway followed depended on the height-to-width ratio of

the small-scale roughness. Additionally, wetting mechanisms through free energy pathways were presented, and the effects of aspect ratio and contact angle were also examined. As a result, a phase diagram showing the possible wetting states was developed. This study provides insight into the design of durable superhydrophobic surfaces (Xin *et al.*, 2024).

1.2 Modelling of interfacial chemistry

The strength of adhesive joints, interface, surface tension and surface energy are important factors. The relative surface plane of solid and liquid phases in contact with each other is defined as the interface. The molecular energies of the solid and liquid phases at the interface are different from the mass energies of the two different phases due to their proximity to each other and as a result of the interaction. Surface tension (γ) is defined as the surface energy per unit area or the force acting per unit length. Surface energy affects the wetting ability of the solid surface of a liquid drop. The total surface energy of a liquid consists of the mass of the liquid and the surface energy of the liquid. In the total surface energy of a system, the Gibbs free surface energy provides the fundamental link between the environmental entropy of the system and the change in heat. In any instant, the Gibbs free energy of a system is obtained by subtracting the product of the entropy change of a system at constant temperature from the enthalpy change of the system.

$$\Delta G^{\circ}: \Delta H^{\circ} - T\Delta S^{\circ}$$

ΔG°: Instantaneous Gibbs free surface energy of a system at any instant

ΔH°: Enthalpy change in the system

T: Constant temperature entropy change in the system

Solid-phase objects can have low or high surface energy. Low-energy surfaces can be brought to a high level with different chemical applications such as primer and anodizing. Thus, the low surface energy phase is absorbed by the high energy phase.

1.3 Surface preparation processes

The adhesion mechanism for adhesive joints depends on the chemical and physical surface properties of the materials to be bonded. Therefore, the key parameter affecting adhesive joints is the interface between the materials. In 1932, a study was conducted by Nicholson (1932) who reported that "to show how a liquid adheres to a solid, it is essential to measure the surface tension of the liquid" (Nicholson, 1932). In adhesive joints, in order to increase the adhesion quality and strength during corrosion, ageing and exposure to environmental external loads, it can be expressed as creating an effective surface microstructure between the existing solid surfaces to be bonded by physical methods such as sandblasting, sanding and chemical interface to increase molecular interaction and surface energy by methods such as primer and anodising, in addition to surface cleaning (Yildiz, Andreopoulos, & Delale, 2019; Ebnesajjad & Ebnesajjad, 2014; Gursel & Cekirge, 2019; Gollins, Chui, Gursel, Delale, & Liaw, 2014; Gursel, 2019). Avila-Sierra, Zhang, and Fryer (2021) noticed that the surface free energy of stainless steel decreases with the accumulation of contamination. Tian, Zou, and Cui (2012) determined that the degree of adhesion of fouling is related to the surface free energy. de Almeida *et al.* (2021) suggested that coating materials with low surface energy have anti-fouling properties, which can reduce frequent cleaning and extend the service life. So, coating the surface of the heat exchanger with high corrosion resistance and high thermal conductivity is the most important approach to solve the fouling and scaling problems. Nevertheless, the relationship between the amount of fouling and surface energy was reported to be irregular (Bohnet, 2003).

1.4 Surface tension and surface energy

All substances in different phases consist of molecules with different forces of attraction. This intermolecular attraction allows different phases to be together. The adhesive attraction force that occurs when a liquid drop spreads in the area where it contacts a solid surface causes the liquid drop to adhere to the solid surface. This is defined as the surface tension of the liquid. The equivalent force of attraction between the molecules on the surface of a solid substance is called surface energy. The area where a liquid phase contacts the solid phase is defined as the interface. Since the molecules of a liquid drop with a high surface tension strongly attract each other, it does not spread on the solid surface, and since the molecules on the solid surface do not tend to attract the liquid molecules, adhesion does not occur at the interface formed by the two phases. On the other hand, the molecules of a liquid drop with low surface tension do not attract each other strongly, so they spread on the solid surface, and the molecules on the solid surface attract the liquid molecules and cause the liquid drop to adhere to the solid surface (Figure 7).

1.5 Wettability, contact angle and spreading

In adhesion theory, the contact angle defines the angle between the gas–liquid interface and the solid–liquid interface. The contact angle of a liquid on a solid surface affects the surface wettability. On surfaces with a high level of wettability, the contact angle decreases, the liquid phase spreads over the solid phase and forms an effective adhesion.

2. Materials and experimental works

2.1 Materials

Steel (Table 1) and (Table 2) and GFRP (Table 3) materials were used in the experiment. Steel specimens were cut from DC01A cold-rolled steel, 0.8 mm (thickness) x 25 mm (width) x

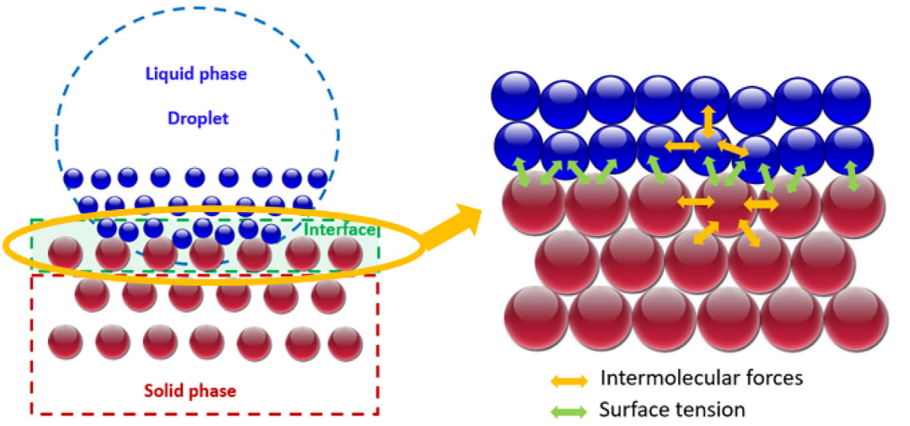

Figure 7. Chemical bonding between molecules. Source: Authors' own work

Table 1. Nominal mechanical properties of DC01 A steel (EN10130)

DC cold-rolled steel (1.0330)	
Max. yield strength (MPa)	280
Tensile strength (MPa)	270–410
Elongation $L_0 = 80$ mm (%)	28

Source(s): Authors' own work

Table 2. Nominal chemical composition of DC01 A steel (EN10130)

C	P	S	Mn	Si	Ti
0.12	0.045	0.045	0.60	–	0.30

Source(s): Authors' own work

Table 3. Nominal mechanical properties of GFRP

Mechanical properties	Value	Unit	Standard
Longitudinal tensile strength, X_t	645	MPa	ISO 527
Transverse tensile strength, Y_t	19.6	MPa	ISO 527
Longitudinal compressive strength, X_c	248	MPa	ISO 527
Transverse compressive strength, Y_c	48.2	MPa	ISO 527
Longitudinal Young's modulus, E_1	37.5	GPa	ISO 527
Transverse Young's modulus strength, E_2	7.32	MPa	ISO 527
Poission's ratio, v_{12}	0.28	–	ISO 527
Poission's ratio, v_{21}	0.05	–	ISO 527
Shear modulus, G_{12}	3.79	GPa	ISO 14129
In-plane shear strength, S_{12}	23.0	MPa	ISO 14129

Source(s): Authors' own work

110 mm (length), used in automotive exterior sheet metal. GFRP specimens were prepared with dimensions of 4 mm (thickness) x 30 mm (width) x 115 mm (length). GFRP composite specimens consisting of glass fibre and epoxy polymer resin were prepared with slightly larger dimensions than steel specimens.

The reason for this is that DC01A steel was laminated into the GFRP material so that the GFRP material does not break from its own structure during the tensile test.

Polyurethane-based, air-curable, one-component Sikaflex-252 (Table 4) was used as the adhesive agent to be used in the experiment. Sika Activator-100 (Table 5) and Sika Primer-206 G + P (Table 6) were used to activate and cure the adhesive in a faster time.

Surface coating preparations of the test specimens: three test specimens were prepared in each different surface group. The GFRP specimen was coated with 30 µm thick polyurethane primer (Table 7) and cured in an oven (Table 8). The coating process and control process complied with ISO2808 and ASTM D3359 standards (Figure 3).

Table 4. Technical specifications of Sikaflex-252

Mechanical properties	Sikaflex-252
Chemical base	1-component polyurethane
Curing mechanism	Moisture curing
Density (Uncured)	1.2 kg/l
Application temperature	10–35 °C
Skin time (CQP019-1)	40 min
Shrinkage (CQP014-1)	5%
Shore A Hardness (CQP023-1/ISO 48–4)	540
Tensile strength (CQP036-1/ISO 527)	3 MPa
Elongation at break (CQP036-1/ISO 37)	400%
Tear propagation resistance (CQP045-1/ISO 34)	7 MPa
Tear lap-shear strength (CQP046-1/ISO 4587)	2,5 MPa
Service temperature (CQP513-1)	130 °C 4h. 150 °C 1h

Source(s): Authors' own work

Table 5. Technical specifications of Sika Activator-100

Technical specifications	Sika Activator-100
Chemical base	Solvent-based ashedion promoter
Consumption	20 ml/mm^2
Flash-off time	≥15 °C 10 min. < 15 °C 30 min
Application temperature	5–40 °C

Source(s): Authors' own work

Table 6. Technical specifications of Sika Primer-206 G + P

Technical specifications	Sika Primer-206 G + P
Chemical base	Solvent-based polyurethane solution
Consumtion	50 ml/mm^2
Flash-off time	≥15 °C 10 min. < 15 °C 30 min. Max. 24 h
Application temperature	5–40 °C

Source(s): Authors' own work

Table 7. Polyurethane based primer paint application conditions

Specifications	Value
Application temperature	25 °C
Relative humidity	60%

Source(s): Authors' own work

Table 8. Polyurethane based primer paint curing condition

Specifications	Value
Curing temperature	80 °C
Curing time	60 min

Source(s): Authors' own work

After shot blasting, three KTL coatings were applied on the steel part using 20 µm thick epoxy resin under application (Table 9) and curing (Table 10) conditions. KTL processes and control were carried out according to ISO 2081 standards (Figure 3).

Table 9. Epoxy based KTL application condition

Specifications	Value
Application temperature	30 °C
Voltage	200 V
Current density	2 A/dm^2
Coating time	4 min
Bath pH	5.5

Source(s): Authors' own work

Table 10. Epoxy based KTL application condition

Specifications	Value
Curing temperature	180 °C
Total curing time	30 min
Oven type	Convection
Air speed	1.5 m/s

Source(s): Authors' own work

The surface roughness of the specimens was measured with the MarSurf PS1 device from ten different regions of the specimens with different surface coatings, and the "Ra" surface roughnesses were measured with the MarSurf PS1 device and are indicated in number order (Table 7) and (Figure 4).

2.2 Experimental works

2.2.1 Preparing of adherends. During the surface coating process of the test specimens, three test specimens were prepared for each different surface group. One group of GFRP specimens was coated with 60 μm thick epoxy primer, another group of GFRP specimens are on the natural material surface without any coating or paint. Cataphoresis coating with a thickness of 20 μm was applied on steel materials.

Measurement of the surface roughness of the samples: "Ra" surface roughnesses of the samples with different surface coatings were measured from ten different regions of the samples with the MarSurf PS1 device and are indicated in number order (Table 11) and (Figure 8).

According to these results, it is seen that the GFRP specimen with a natural surface ranks first. The GFRP specimen coated with a pigment-based primer ranks second in the surface roughness classification. The surface roughness of the KTL-coated steel surface is lower than that of both GFRP specimens.

Bonding of substrates, moulds prepared according to the adhesive thickness were used for bonding the specimens (substrate), steel and GFRP parts (Figure 9a). The surfaces were then cleaned with scotchbrite. Then Sika activator-100 was applied with a melamine sponge and allowed to dry for 10 min. Next, Sika primer-206 G + P was applied on the dried activator and allowed to dry for 15 min (Figure 9b). Finally, the substrates were bonded with each other in a single lap joint type using Sikaflex-252 polyurethane adhesive at appropriate adhesive thicknesses (Figure 9c) and allowed to cure at room conditions (Figure 9d).

Table 11. Surface measurement values of samples with different surface coatings

Sample type	Surface roughness measurements; R_a 1	2	3	4	5	6	7	8	9	10	Avg.
Natural GFRP surface	5.382	5.710	5.903	6.654	6.864	7.852	7.975	8.154	8.699	8.998	7.219
Primer painted GFRP surface	1.304	1.309	1.315	1.326	1.362	1.460	1.486	1.506	1.533	1.579	1.418
KTL-coated steel	0.318	0.320	0.324	0.326	0.327	0.332	0.335	0.341	0.349	0.354	0.334

Source(s): Authors' own work

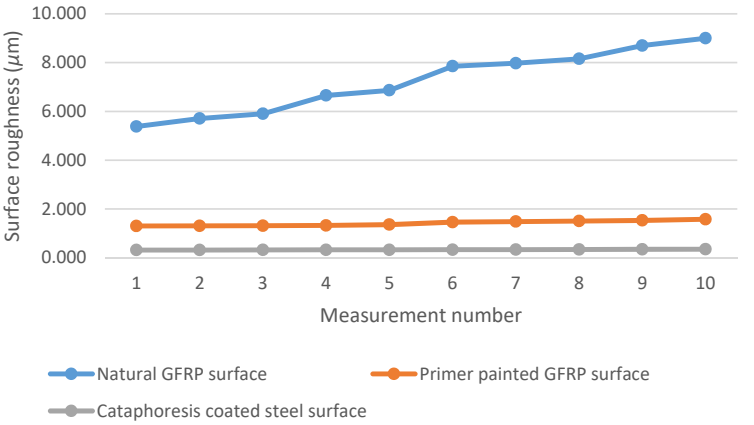

Figure 8. Surface roughness values of samples with different surface coatings. Source: Authors' own work

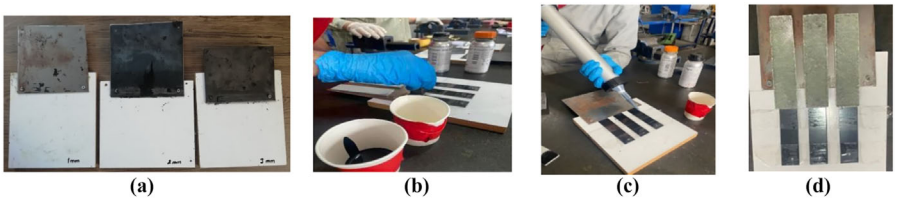

Figure 9. Application steps of bonding process. Source: Authors' own work

2.2.2 Tensile test. Tensile tests were conducted under ambient conditions in accordance with the ASTM D1002 standard, which specifies the method for determining the shear strength of single-lap joints (Figure 10) bonded joints under tensile test parameters (Table 12).

A total of nine tensile tests were performed at the specified parameters, with three specimens prepared for each group with different surface coatings (Table 9).

Based on the adhesive thicknesses of the KTL coated steel part and the GFRP part without any coating on the surface, the tensile test results of the specimens prepared by single lap jointing were obtained (Table 13 and Figure 11). Three specimens were tested for each thickness.

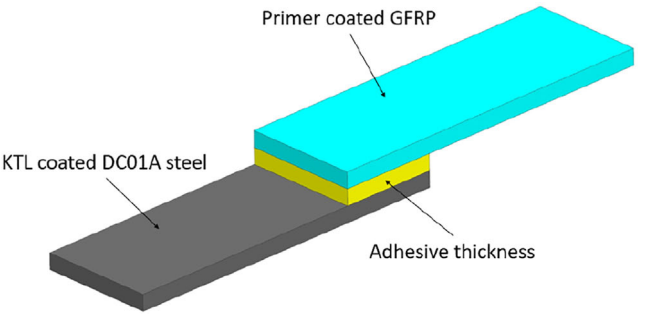

Figure 10. GFRP and steel part joined as a single lap joining type. Source: Authors' own work

Table 12. Tensile test parameters used in the experiment

Test parameters	Value
Pre-load	2 MPa
Speed, E-Modulus	20 MPa/s
Speed Rp, ReH	60 MPa/s
Speed in yield range	0.002 s^{-1}
Test speed	0.005 s^{-1}

Source(s): Authors' own work

Table 13. Tensile test values of uncoated GFRP parts according to adhesive thicknesses

Ultimate stress Adhesive thickness	R_m (MPa) 1 mm	2 mm	3 mm
Sample-1	10	11	6
Sample-2	5	7	5
Sample-3	4	6	4

Source(s): Authors' own work

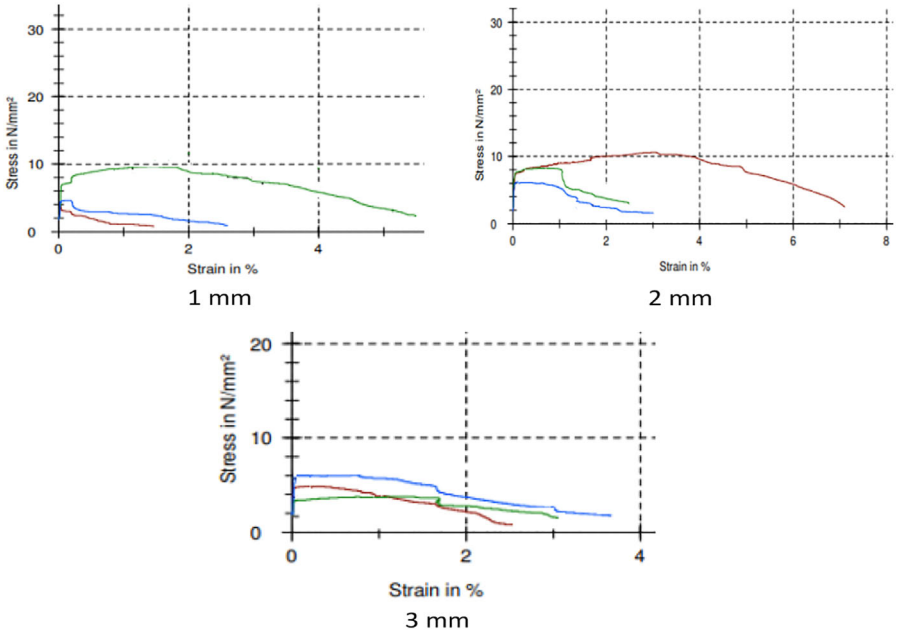

Figure 11. Tensile test results of uncoated GFRP parts according to bonding thickness. Source: Authors' own work

The tensile test results of the specimens prepared by single lap jointing based on the adhesive thicknesses of the KTL steel part and the GFRP part with primer painted surface were obtained (Table 14 and Figure 12). Three specimens were tested for each thickness.

Table 14. Tensile test values of primer coated GFRP parts according to adhesive thicknesses

Ultimate stress Adhesive thickness	R_m (MPa) 1 mm	2 mm	3 mm
Sample-1	22	19	16
Sample-2	18	17	13
Sample-3	19	16	12

Source(s): Authors' own work

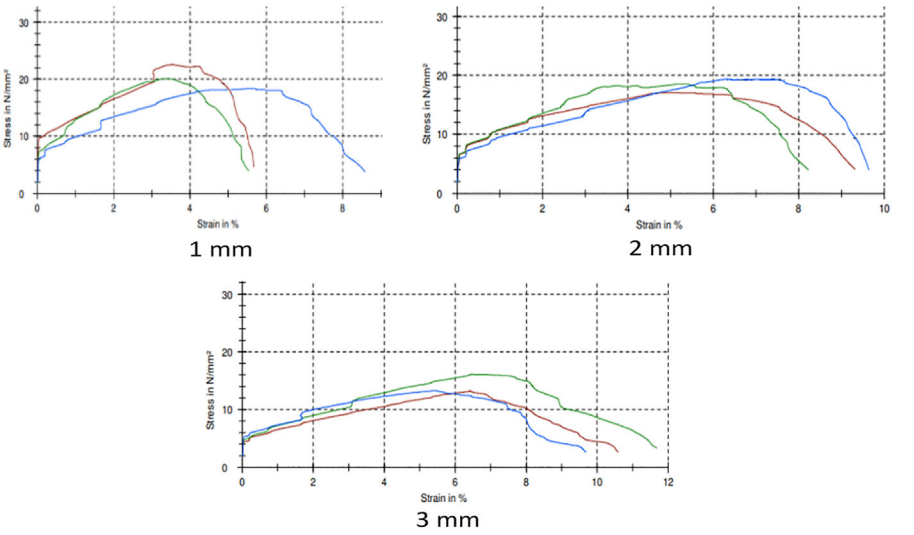

Figure 12. Tensile test results of primer coated GFRP parts according to bonding thickness. Source: Authors' own work

In order to explain the effect of different adhesive thicknesses and surface combinations on the tensile strength, the average tensile test results of the test specimens with different surfaces (Table 15) were visualised with Python software (Figure 13).

Natural GFRP + KTL-coated steel (Type 1): Tensile strength is between 5 and 7 MPa. As the thickness increased, a decrease in tensile strength was observed. In this case, the increase in adhesive thickness is not an effective factor on the bond strength.

Table 15. Average tensile test values of primer coated GFRP parts according to adhesive thicknesses

Adhesive bonding thickness	1 mm	2 mm	3 mm	1 mm	2 mm	3 mm
Rm ultimate tensile strength (MPa)	6	7	5	20	17	12
Adherends type	(a) Natural surface of GFRP + KTL coated steel			(b) Primer painted GFRP + KTL coated steel		

Source(s): Authors' own work

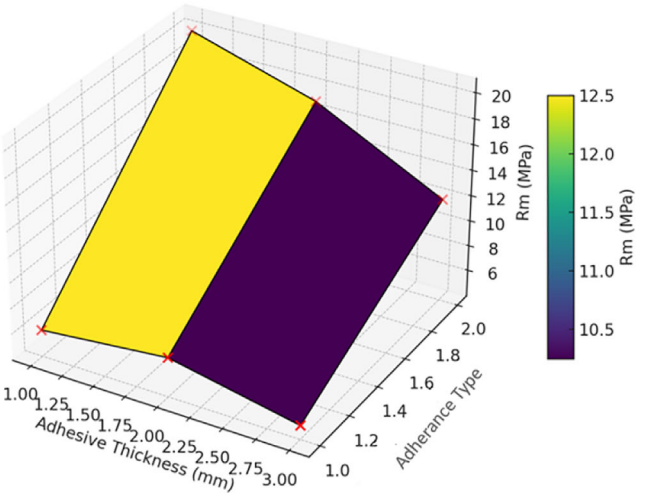

Figure 13. Farklı yüzeylerde yüzey pürüzlülüğü, yapıştırma kalınlığı ilişkisi. Source: Authors' own work

Primer painted GFRP + KTL-coated steel (Type 2): Tensile strength is between g12 and 20 MPa. It is noticeably increased compared to the other type. This shows that surface preparation greatly improves the bond strength. The primer coating increases the surface energy and ensures better wetting of the adhesive. This directly increases the bond strength.

Adhesive thickness is not optimum for both groups; too thick or too thin reduces performance. Especially 2 mm thickness gives the best results for Type 1, while the best value is seen at 1 mm in Type 2.

2.2.3 Optical microscope investigation. Optical microscope examination of the specimen surfaces after the tensile test provides information about the adhesion strength of the surface properties. In the test specimen formed with GFRP without any coating and paint on the surface (natural surface) (Figure 14a) and KTL-coated steel surface (Figure 14b), almost 100% adhesive failure was realised on the GFRP surface as a result of the tensile test. Most of the adhesive peeled off on the GFRP surface. But, in KTL-coated steel, the adhesive remained on the surface and was detected as cohesive failure.

KTL coated steel and primer painted GFRP specimens; it was observed that the adhesive agent peeled off from the natural surface GFRP material with the highest roughness value. Therefore, the wetting ability of the bonding zone was low and cohesive failure was detected. In the specimen formed with primer-painted GFRP (Figure 14c) and KTL-coated steel surface (Figure 14d), the tensile test showed that the adhesive peel-off was less on the primer-painted GFRP surface.

3. Discussion and results

GFRP is an increasingly preferred composite material in the railway sector due to its advantages, such as lightness, durability and corrosion resistance. This material provides long-lasting components with high fatigue resistance and improves transportation efficiency by reducing fuel consumption. However, its performance is limited at high temperatures, so heat-resistant versions should be preferred. Additionally, the thermal expansion coefficient of GFRP differs from that of metals, which should be considered in the design. Wear resistance can be enhanced with the right resin and fibre structure, providing durability in surfaces like braking systems. GFRP is more resistant to chemical environments and corrosion compared to metal materials. However, its impact resistance may be lower, so reinforcing fibres can be used

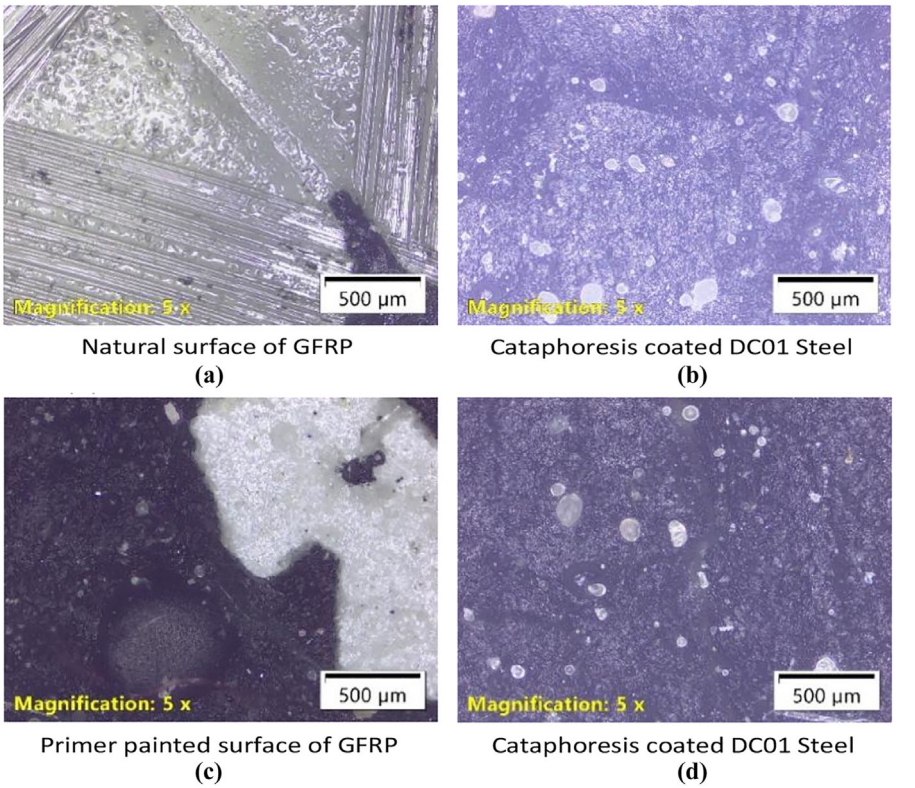

Figure 14. Optical microscope surface images of different materials with different surface properties. Source: Authors' own work

in the design. While its production is more complex than traditional metal materials, it can be cost-effective for large structures. Overall, the advantages of GFRP lead to reduced maintenance and operating costs, making it an effective material choice for railway transportation systems.

To protect steel structures from corrosion, a primer coating is commonly applied as part of the manufacturing process. Accordingly, the adhesion strength between GFRP composite materials and primer-coated steel surfaces becomes a crucial consideration in maintaining the structural integrity and durability of bonded assemblies.

Although it is common to apply primer paint to steel surfaces prior to the adhesive bonding process, this research suggests that cataphoresis coating of steel surfaces is an alternative solution. The research further demonstrates that cataphoresis not only enhances corrosion resistance but also serves as an effective chemical pre-treatment for improving the performance of adhesive joints.

In addition, the influence of adhesive thickness and surface roughness on bond strength was analysed. Results showed that increasing either the adhesive layer thickness or surface roughness did not lead to improved bonding performance when the roughness exceeded an optimal threshold. This suggests that excessive surface texturing may not be beneficial and that there exists an optimum surface condition for maximizing adhesive strength.

Overall, the study highlights the critical role of surface treatment in the adhesion performance of GFRP-to-steel joints and confirms that cataphoresis coating presents a promising alternative to traditional primer applications in railway manufacturing.

4. Conclusion

The present study emphasizes the critical importance of primer application on the adhesive surfaces of glass fibre-reinforced polymer (GFRP) composites to achieve strong and reliable adhesive bonding with cataphoresis (KTL)-coated steel substrates. This finding is particularly relevant in the context of structural bonding in transportation applications, where the integrity of adhesive joints is essential.

Experimental investigations revealed that GFRP composite surfaces without any chemical surface treatment – characterized by a pronounced and deep surface roughness – failed to provide adequate mechanical interlocking. Among all the tested configurations, natural GFRP samples with deep surface roughness exhibited the lowest bond strength. This poor adhesion performance can be attributed to the inability of the adhesive to effectively penetrate and wet such excessively rough surfaces. At these roughness levels, the spreadability of the adhesive is significantly reduced, which limits its contact area with the substrate, resulting in insufficient wetting and poor interfacial bonding. This situation shows that the adhesive agent does not fully penetrate the surface and remains suspended on the surface, as stated in the *Cassey–Baxter theorem*.

In contrast, GFRP specimens coated with a suitable primer showed significantly improved adhesion to KTL-coated steel substrates. This result suggests that the inherent surface energy of such untreated GFRP is relatively low, which adversely affects the ability of the adhesive to wet out and adhere effectively. Primer application significantly increases the surface energy of GFRP materials, thus promoting better adhesive wetting and spreading behaviour. As a result, a much stronger interfacial interaction is established between the primer-coated GFRP surface and the cataphoresis-coated steel as described in *Wenzel's theorem*, the adhesive agent spreads over the entire surface and the wetting ability increases. This results in higher adhesive bond strength.

In conclusion, the application of a primer layer to cathodically coated steel surfaces has been shown to significantly improve the adhesive bonding performance with GFRP composite materials. Experimental results reveal that primed joints achieve a shear strength of approximately 20 MPa, which is about 300% higher than their unprimed counterparts. Additionally, it has been observed that moderate surface roughening improves adhesion, while excessive roughening may hinder bond formation. These findings highlight that the cataphoresis coating process not only enhances corrosion resistance but also significantly improves the adhesive bonding performance of hybrid material joints. Furthermore, this process offers a promising strategy for improving the reliability and long-term durability of adhesive joints, particularly in the manufacturing of railway vehicles, where bonding of steel and GFRP components is crucial.

References

Akniyet, A., Essam, S., Arshyn, M., Aidar, S., Serik, T., & Shoaib, S. (2022). Challenges and opportunities of implementing Industry 4.0 in recycling carbon fiber reinforced composites. *Advanced Science and Technology, 6626*, 67–73. doi: 10.4028/p-3zmq61.

Alachek, I., Reboul, N., & Jurkiewiez, B. (2019). Experimental and finite element analysis of the long-term behaviour of GFRP-concrete hybrid beams fabricated using adhesive bonding. *Composite Structures, 207*, 148–165. doi: 10.1016/j.compstruct.2018.09.013.

Ardila-Rodríguez, L. A., Boshuizen, B., Rans, C., & Poulis, J. A. (2021). The influence of grit blasting and UV/Ozone treatments on Ti-Ti adhesive bonds and their durability after sol-gel and primer application. *International Journal of Adhesion and Adhesives, 104*, 102750. doi: 10.1016/j.ijadhadh.2020.102750.

Avila-Sierra, A., Zhang, Z. Y. J., & Fryer, P. J. (2021). Effect of surface roughness and temperature on stainless steel-whey protein interfacial interactions under pasteurisation conditions. *Journal of Food Engineering, 301*, 110542. doi: 10.1016/j.jfoodeng.2021.110542.

Banea, M. D., & Da Silva, L. F. M. (2009). Adhesively bonded joints in composite materials: An overview. *Proceedings of the Institution of Mechanical Engineers, Part L: Journal of Materials: Design and Applications, 223*, 1–18. doi: 10.1243/14644207JMDA219.

Barnes, T. A., & Pashby, I. R. (2000). Joining techniques for aluminium spaceframes used in automobiles Part II - adhesive bonding and mechanical fasteners. *Journal of Materials Processing Technology*, *99*, 72–79. doi: 10.1016/S0924-0136(99)00361-1.

Baykara, C. (2023a). Effects of single-lap joint at different adhesive thicknesses on fatigue strength of metals with different surface coatings. *Proceedings of the Institution of Mechanical Engineers – Part C: Journal of Mechanical Engineering Science*, *237*(17), 3987–4004. doi: 10.1177/09544062231152995.

Baykara, C. (2023b). The effect of adhesive strength on thin-walled metal surfaces coated with cataphoresis application according to adhesive thickness. In L. F. M. da Silva & R. D. Adams (Eds.). *Proceedings of the 7th International Conference on Structural Adhesive Bonding*, Cham: Springer (p. 7). doi: 10.1007/978-3-031-48363-9.

Baykara, C. (2024). Farklı Kimyasal Yöntemlerle Kaplanmış Çelik Plakaların Farklı yapıştırma Kalınlıklarda Tek Bindirmeli Birleştirme Yöntemiyle Birleştirilen Numunelerin Yorulma Analizleri Sonuçlarının Wöhler Eğrilerinde Karşılaştırılması. *Afyon Kocatepe Üniversitesi Fen ve Mühendislik Bilimleri Dergisi*, *24*(1), 176–188. doi: 10.35414/akufemubid.1288047.

Baykara, C., Teke, I. T., & Ertas, A. H. (2023). Effects of the single-lap joint on fatigue strength of metals with different surface coatings: A numerical simulation. *E3S Web of Conferences*, *402*, 7. doi: 10.1051/e3sconf/202340211011.

Bi, X., Wang, Z., Xu, M., & Li, X. (2022). Femtosecond laser fabricated micro/nano interfacial structures to strengthen CFRPEEK/A6061-T6 FLJ hybrid joints. *Composites Part B: Engineering*, *231*, 109540. doi: 10.1016/j.compositesb.2021.109540.

Blohowiak, K. Y., Osborne, J. H., & Krienke, K. A. (1998). Sol for coating metals. U.S. Patent No. 5,814,137.

Bohnet, M. (2003). Influence of the transport properties of the crystal/heat transfer surface interfacial on fouling behavior. *Chemical Engineering and Technology*, *26*(8), 1055–1060. doi: 10.1002/ceat.200301807.

Callinan, R. J., & Galea, S. C. (2002). Advances in the bonded composite repair of metallic aircraft structure, *2*. doi: 10.1016/B978-008042699-0/50021-8.

Cao, J., Gao, D., Li, C., Si, X., Jia, J., & Qi, J. (2021). Bioinspired metal-intermetallic laminated composites for the fabrication of superhydrophobic surfaces with responsive wettability. *ACS Applied Materials and Interfaces*, *13*(5), 5834–5843. doi: 10.1021/acsami.0c20639.

Cobb, T. Q., Johnson, W. S., Lowther, S. E., & St Clair, T. L. (1999). Optimization of surface treatment and adhesive selection for bond durability in Ti-15-3 laminates. *Journal of Adhesion*, *71*(2-3), 115–141. doi: 10.1080/00218469908014844.

Correia, S., Anes, V., & Reis, L. (2018). Effect of surface treatment on adhesively bonded aluminium-aluminium joints regarding aeronautical structures. *Engineering Failure Analysis*, *84*, 34–45. doi: 10.1016/j.engfailanal.2017.10.010.

de Almeida, C. F., Saget, M., Delaplace, G., Jimenez, M., Fierro, V., & Celzard, A. (2021). Innovative fouling-resistant materials for industrial heat exchangers: A review. *Reviews in Chemical Engineering*, *39*(1), 71–104. doi: 10.1515/revce-2020-0094.

Ebnesajjad, S., & Ebnesajjad, C. (2014). Surface treatment of materials for adhesive bonding. In *Adhesives Technology Handbook*, Elsevier (pp. 3–24).

Extrand, C. W. (2002). Model for contact angles and hysteresis on rough and ultraphobic surfaces. *Langmuir*, *18*(21), 7991–7999. doi: 10.1021/la025769z.

Farley, G. L. (1983). Energy absorption of composite materials. *Journal of Composite Materials*, *17*(3), 267–279. doi: 10.1177/002199838301700307.

Fischer, F., Kreling, S., Jäschke, P., Frauenhofer, M., Kracht, D., & Dilger, K. (2012). Laser surface pre-treatment of CFRP for adhesive bonding in consideration of the absorption behaviour. *Journal of Adhesion*, *88*(4-6), 350–363. doi: 10.1080/00218464.2012.660042.

Fu, J., Liu, Q., Liufu, K., Deng, Y., Fang, J., & Li, Q. (2019). Design of bionic-bamboo thin-walled structures for energy absorption. *Thin-Walled Structures*, *135*, 400–413. doi: 10.1016/j.tws.2018.10.003.

Fuertes, T., Kruse, T., Koerwien, T., & Geistbeck, M. (2015). Bonding of CFRP primary aerospace structures – Discussion of the certification boundary conditions and related technology fields addressing the needs for development. *Composite Interfaces*, *22*(8), 795–808. doi: 10.1080/09276440.2015.1077048.

Ghasemlou, M., Daver, F., Ivanova, E. P., & Adhikari, B. (2019). Bio-inspired sustainable and durable superhydrophobic materials: From nature to market. *Journal of Materials Chemistry, A*(28), 16643–16670. doi: 10.1039/c9ta05185f.

Ghumatkar, A., Sekhar, R., & Budhe, S. (2017). Experimental study on different adherend surface roughness on the adhesive bond strength. *Materials Today: Proceedings*, *4*(8), 7801–7809. doi: 10.1016/j.matpr.2017.07.115.

Gollins, K., Chui, J., Gursel, A., Delale, F., & Liaw, B. M. (2014). Comparison of manufacturing techniques subject to high speed impact. In *ASME 2014 International Mechanical Engineering Congress and Exposition (IMECE2014-39677)*, Montreal, Canada.

Goudarzi, R. H., & Khedmati, M. R. (2020). An experimental and numerical investigation of adhesive bond strength in Al-GFRP single lap and double butt lap joints due to applied longitudinal loads. *Ships and Offshore Structures*, *15*(4), 403–416. doi: 10.1080/17445302.2019.1659879.

Greenwood, J. A., & Williamson, J. B. P. (1966). Contact of nominally flat surfaces. *Proceedings of the Royal Society of London. Series A: Mathematical and Physical Sciences*, *295*, 300–319. doi: 10.1098/rspa.1966.0242.

Guadagno, L., Sarno, M., Vietri, U., Raimondo, M., Cirillo, C., & Ciambelli, P. (2015). Graphene-based structural adhesive to enhance adhesion performance. *RSC Advances*, *5*(35), 27874–27886. doi: 10.1039/C5RA00819K.

Guo, L., Liu, J., Xia, H., Li, X., Zhang, X., & Yang, H. (2021). Effects of surface treatment and adhesive thickness on the shear strength of precision bonded joints. *Polymer Testing*, *94*, 107063. doi: 10.1016/j.polymertesting.2021.107063.

Gursel, A. (2019). Fundamentals in adhesive bonding design for complex structures and conditions. *Journal of Advanced Technology Sciences*, *8*(1), 1–10.

Gursel, A., & Cekirge, H. M. (2019). Adhesive joints subjected to impact loading: A review. *International Journal of Materials Engineering*, *9*(1), 16–21. doi: 10.5923/j.ijme.20190901.03.

He, P., Chen, K., Yu, B., Yue, C. Y., & Yang, J. (2013). Surface microstructures and epoxy bonded shear strength of Ti6Al4V alloy anodized at various temperatures. *Composites Science and Technology*, *83*, 15–22. doi: 10.1016/j.compscitech.2013.04.007.

He, P., Huang, M., Fisher, S., Yue, C. Y., & Yang, J. (2015). Effects of primer and annealing treatments on the shear strength between anodized Ti6Al4V and epoxy. *International Journal of Adhesion and Adhesives*, *57*, 49–56. doi: 10.1016/j.ijadhadh.2014.10.004.

Hejazi, V., Moghadam, A. D., Rohatgi, P., & Nosonovsky, M. (2014). Beyond Wenzel and Cassie–Baxter: Second-order effects on the wetting of rough surfaces. *Langmuir*, *30*(31), 9423–9429. doi: 10.1021/la502143v.

Huré, M., Olivier, P., & Garcia, J. (2022). Effect of Cassie-Baxter versus Wenzel states on ice adhesion: A fracture toughness approach. *Cold Regions Science and Technology*, *194*, 103440. doi: 10.1016/j.coldregions.2021.103440.

Jiang, Y., & Choi, C. (2020). Droplet retention on superhydrophobic surfaces: A critical review. *Advanced Materials Interfaces*, *8*(1), 2001205. doi: 10.1002/admi.202001205.

Khaskhoussi, A., Calabrese, L., & Proverbio, E. (2022). Anticorrosion superhydrophobic surfaces on AA6082 aluminum alloy by HF/HCl texturing and self-assembling of silane monolayer. *Materials*, *15*(23), 8549. doi: 10.3390/ma15238549.

Kim, S., Kim, D. H., Su, H. C., Woo, Y. K., Sin, K., & Young, T. C. (2020). Effect of surface pattern morphology on inducing superhydrophobicity. *Applied Surface Science*, *513*, 145847. doi: 10.1016/j.apsusc.2020.145847.

Kreling, S., Fischer, F., Delmdahl, R., Gäbler, F., & Dilger, K. (2013). Analytical characterization of CFRP laser treated by excimer laser radiation. *Physics Procedia*, *41*, 282–290. doi: 10.1016/j.phpro.2013.03.080.

Lin, Y., Qian, W., Lei, L., Liu, Y., Zhang, J., Liu, J., … Wu, S. (2025). Structural integrity issues of composite materials and structures in future transportation equipment. *Composite Structures*, *358*, 118943. doi: 10.1016/j.compstruct.2025.118943.

Liu, J., Wang, W., Yan, Y., He, H., Xue, Z., Xu, C., & Li, L. (2022). Influence of raw material surface roughening on the lap shearing strength and failure behavior of adhesively bonded aluminum joints. *International Journal of Advanced Manufacturing Technology*, *122*(1), 327–342. doi: 10.1007/s00170-022-09590-6.

Mamalis, A. G., Manolakos, D. E., Ioannidis, M. B., & Papapostolou, D. P. (2004). Crashworthy characteristics of axially statically compressed thin-walled square CFRP composite tubes: Experimental. *Composite Structures*, *63*(3-4), 347–360. doi: 10.1016/S0263-8223(03)00183-1.

McHale, G. (2007). Cassie and Wenzel: Were they really so wrong?. *Langmuir*, *23*(15), 8200–8205. doi: 10.1021/la7011167.

Molitor, P., Barron, V., & Young, T. (2001). Surface treatment of titanium for adhesive bonding to polymer composites: A review. *International Journal of Adhesion and Adhesives*, *21*(2), 129–136. doi: 10.1016/S0143-7496(00)00044-0.

Moreira, R., Oliveira, V., Silva, F., Vilar, R., & Moura, M. (2018). Mode II fracture toughness of carbon-epoxy bonded joints with femtosecond laser treated surfaces. *International Journal of Mechanical Sciences*, *148*, 707–713. doi: 10.1016/j.ijmecsci.2018.09.029.

Nicholson, V. (1932). Adhesion tension in asphalt pavements, its significance and methods applicable in its determination. *Journal of the Association of Asphalt Paving Technologists*, *3*, 28–49. doi: 10.14295/transportes.v28i2.2071.

Nidhal, N., Yasmina, B., Sami, N., Salah, M., & Martins, D. S. L. F. (2023). Effect of surface texture on the mechanical performance of bonded joints: A review. *Journal of Adhesion*, *99*(2), 166–258. doi: 10.1080/00218464.2021.2008370.

Oliveira, V., Moreira, R., Moura, M., & Vilar, R. (2018). Surface patterning of CRFP composites using femtosecond laser interferometry. *Applied Physics A*, *124*(3), 231. doi: 10.1007/s00339-018-1662-x.

Ostapiuk, M., & Bienias, J. (2020). Fracture analysis and shear strength of aluminum/CFRP and GFRP adhesive joint in fiber metal laminates. *Materials*, *13*(7), 7. doi: 10.3390/ma13010007.

Ozgür, B., Erhan, A., Onur, Ç., Belgin, G., & Arif, D. (2018). The effect of CO2 laser-induced microhole formations on adhesive bonding strength of CFRP/CFRP joints. *Polymer Composites*, *40*(7), 2891–2900. doi: 10.1002/pc.25119.

Palomba, G., Epasto, G., & Crupi, V. (2021). Lightweight sandwich structures for marine applications: A review. *Mechanics of Advanced Materials and Structures*, *29*(26), 4839–4864. doi:10.1080/15376494.2021.1941448.

Park, I. W., Ribe, J. M., Fernandino, M., & Dorao, C. A. (2023). The criterion of the Cassie–Baxter and Wenzel wetting modes and the effect of elastic substrates on it. *Advanced Materials Interfaces*, *10*(12), 2202439. doi: 10.1002/admi.202202439.

Pethrick, R. A. (2015). Design and aging of adhesives for structural adhesive bonding–A review. *Proceedings of the Institution of Mechanical Engineers, Part L: Journal of Materials: Design and Applications*, *229*(5), 349–379. doi: 10.1177/1464420714522981.

Price, J., & Hull, D. (1987). Axial crushing of glass fibre-polyester composite cones. *Composites Science and Technology*, *28*(3), 211–230. doi: 10.1016/0266-3538(87)90003-0.

Rajak, D. K., Pagar, D. D., Kumar, R., & Pruncu, C. I. (2019). Recent progress of reinforcement materials: A comprehensive overview of composite materials. *Journal of Materials Research and Technology*, *8*(6), 6354–6374. doi: 10.1016/j.jmrt.2019.09.068.

Rauter, M. T., Schnell, S. K., & Kjelstrup, S. (2021). Cassie–baxter and Wenzel states and the effect of interfaces on transport properties across membranes. *Journal of Physical Chemistry B*, *125*(46), 12730–12740. doi: 10.1021/acs.jpcb.1c07931.

Rudawska, A., & Wahab, M. A. (2019). The effect of cataphoretic and powder coatings on the strength and failure modes of EN AW-5754 aluminium alloy adhesive joints. *International Journal of Adhesion and Adhesives*, *89*, 40–50. doi: 10.1016/j.ijadhadh.2018.11.005.

Sudeepthi, A., Yeo, L., & Sen, A. K. (2020). Cassie–Wenzel wetting transition on nanostructured superhydrophobic surfaces induced by surface acoustic waves. *Applied Physics Letters*, *116*(9), 093704. doi: 10.1063/1.5145282.

Tian, X. J., Zou, Y., & Cui, H. Y. (2012). A study of the anti-fouling property of the electroless Ni-P-Sn coating. *Advanced Materials Research*, *538-541*, 538–541, 218–221. doi: 10.4028/www.scientific.net/AMR.538-541.218.

Wang, H., Hao, X., Zhou, H., Li, D., & Hua, L. (2016). Study on ultrasonic vibration-assisted adhesive bonding of CFRP joints. *Journal of Adhesion Science and Technology*, *30*(17), 1842–1857. doi: 10.1080/01694243.2016.1168338.

Wui, H., Tong, X., Chen, Y., Hua, L., Wu, M., & Ji, W. (2021). Study on ultrasonic vibration-assisted adhesive bonding of CFRP laminates with laser ablation-treated surfaces. *Composite Structures*, *268*, 113983. doi: 10.1016/j.compstruct.2021.113983.

Xin, H., Fan, J., Cui, K., Tian, Y., Wang, T., & Wang, S. (2024). Wetting of nanoscale water films on hierarchically structured surfaces. *Physics of Fluids*, *36*(5), 052016. doi: 10.1063/5.0205294.

Xin He, X., Zhang, B. X., Wang, S. L., Wang, Y. F., Yang, Y. R., Wang, X. D., & Lee, D. L. (2021). The Cassie-to-Wenzel wetting transition of water films on textured surfaces with different topologies. *Physics of Fluids*, *33*(11), 112006. doi: 10.1063/5.0066106.

Yildiz, S., Andreopoulos, Y., & Delale, F. (2019). Mode I characterization of toughened epoxy adhesive joints under shock-wave loading. *International Journal of Adhesion and Adhesives*, *90*, 71–87. doi: 10.1016/j.ijadhadh.2019.03.017.

Yuan, Y., Guo, X., He, H., Zhang, K., & Han, W. (2024). Rapid surface patterning to strengthen adhesive bonding of carbon fiber reinforced polymer by spatial shaping femtosecond laser. *Optics and Laser Technology*, *180*, 111562. doi: 10.1016/j.optlastec.2024.111562.

Zamani, P., Jaamialahmadi, A., da Silva, L. F. M., & Farhangdoost, K. (2019). An investigation on fatigue life evaluation and crack initiation of Al-GFRP bonded lap joints under four-point bending. *Composite Structures*, *229*, 111433. doi: 10.1016/j.compstruct.2019.111433.

Zamani, P., Jaamialahmadi, A., & Da Silva, L. F. M. (2023). Fatigue life evaluation of Al-GFRP bonded lap joints under four-point bending using strain-life criteria. *International Journal of Adhesion and Adhesives*, *122*, 103338. doi: 10.1016/j.ijadhadh.2022.103338.

Zhang, J. -S., Zhao, X. -H., Zuo, Y., & Xiong, J. -P. (2008). The bonding strength and corrosion resistance of aluminum alloy by anodizing treatment in a phosphoric acid modified boric acid/sulfuric acid bath. *Surface and Coatings Technology*, *202*(14), 3149–3156. doi: 10.1016/j.surfcoat.2007.10.041.

Zhang, Z., Shan, J., Tan, X., & Zhang, J. (2017). Improvement of the laser joining of CFRP and aluminum via laser pre-treatment. *International Journal of Advanced Manufacturing Technology*, *90*(9-12), 3465–3472. doi: 10.1080/09276440.2015.1077048.

Corresponding author
Celalettin Baykara can be contacted at: cbaykara@subu.edu.tr

Dr. Celalettin Baykara graduated from the Faculty of Engineering, Department of Mechanical Engineering at Eastern Mediterranean University in 1995 in North Cyprus. He completed his master's degree in the field of materials at Celal Bayar University in 1998 in Manisa-Turkiye. In 2005, he obtained his Ph.D. in welding from Sakarya University in Sakarya-Turkiye. His academic career has progressed in parallel with his professional work experience. Between 1996 and 2011, he held engineering positions at companies such as MAN Turkey and Hyundai Assan. As part of his professional duties, he served as a manager in countries including China, India, the United Kingdom, Egypt, and Mexico. In 2018, he transitioned to a public university. With his industry experience, he is specialized in the fields of mechanics, materials, and manufacturing methods. He is currently continuing his academic career at Sakarya University of Applied Sciences.